Springer

Journal of
Mechanical
Science and
Technology

Journal of Mechanical Science and Technology 22 (2008) 740~745

www.springerlink.com/content/1738-494x

Interferometric measurement using bimorph actuated staggered mirror (BASM) microsensor

Si-Hyung Lim* and Hong Jae Yim

School of Mechanical and Automotive Engineering, Kookmin University Jeongneung-dong, Sungbuk-gu, Seoul, Korea

(Manuscript Received June 28, 2007; Revised August 17, 2007; Accepted August 17, 2007)

Abstract

For physical and chemical sensing applications, a bimorph actuated staggered mirror (BASM) microsensor was designed and fabricated by surface micromachining using a transparent quartz substrate. While the conventional cantilever sensors have angular deflection, BASM's moving mirror performs piston-type pure vertical motion in response to environmental stimuli like temperature change and surface stress change due to molecular adsorption. Since the sensor itself has a fixed or reference mirror as well as a moving mirror, 1) an interferometric measurement is possible without an additional reference mirror in off-axis measurement setup, and 2) vibration measurement noise can be reduced. For preliminary test purposes, interferometric measurement using an optical setup was performed for temperature change. At He-Ne line (632.8 nm), a temperature change of ~0.8 K caused a minimum-to-maximum interferometric light intensity change which corresponds to ~144 nm shift of the moving mirror part. An optical diffraction analysis was performed and optimal device parameters were found to maximize the sensor sensitivity.

Keywords: Interferometry; Bimorph; Physical sensor; Chemical sensor; Micro mirror; Optical diffraction

1. Introduction

Microcantilever sensors have been extensively used for physical [1], chemical [2-11], and biological [1, 12-16] detection. A cantilever sensor deflects due to physically or chemically induced surface stress. Although there are a number of signal transduction methods like optical, piezoresistive, capacitive, and piezoelectric, the most common readout techniques for cantilever deflection measurement are optical, including optical lever and interferometric methods. The optical sensing method can detect cantilever motion with sub-Angstrom resolution, limited only by thermal vibrational noise of the cantilever [1, 17].

Interferometric measurement of cantilever sensors has been used for thermal imaging [1], acceleration [18, 19], chemical sensing [10], biological sensing [20], etc. Typically, comb structures are attached to the end of two cantilevers (one is fixed and the other is moving). Relative bending motion (angular and vertical component) between two mirrors generates a diffraction pattern and light intensity change of a specific diffraction order mode.

In the previous work [21], a staggered mirror microsensor, which can be operated by temperature change and surface stress change due to molecular adsorption was proposed. Also, its nanometer scale pure vertical motion demonstrated. For higher sensitivity, a novel structure, or FOB (Flip-Over Bimaterial) beam, was proposed. It has a configuration such that a material layer coats the top and bottom of the second material at different regions along the beam length. By multiple interconnections of the FOB beams, the deflection or sensitivity could be amplified. It should be noted that due to its symmetric structure our BASM microsensor performs piston-type pure vertical motion, which is different from the bending

*Corresponding author. Tel.: +82 2 910 4672, Fax.: +82 2 910 4839
E-mail address: shlim@kookmin.ac.kr
DOI 10.1007/s12206-007-1030-9

motion in cantilever sensors using comb structures. The pure vertical motion of a sensing structure offers a potential for high sensitivity interferometric measurement.

In this work, using an interferometric setup, the changes in light intensity due to the temperature change were measured in the ambience of the BASM chip. Also, an optical diffraction analysis was performed to maximize the optical sensitivity.

2. Interferometric measurement

As shown in Fig. 1(a), the BASM microsensor (100 μm×100 μm) consists of a quartz substrate, an aluminum fixed mirror (attached to the quartz substrate surface), a gold moving mirror (attached to the bottom of the middle moving section; 52 μm×52 μm), symmetric bimorph sensing legs (left and right side; single leg length 100 μm and width 3 μm), etc. The middle moving part performs piston-type pure vertical motion for temperature change and molecular adsorption. Thermal deformation is caused by the thermal expansion mismatch between the two different materials. On the other hand, surface stress deformation is generated by the equilibrium between chemical and mechanical free energies during molecular adsorption or interaction [22]. Fig. 1(b) shows the top-view optical micrographs of the chip. Focuses change from the chip substrate to the middle part. The middle part (the moving mirror is attached to its bottom side) has an initial deflection of ~13 μm from the chip substrate, which comes from the residual stress of bimorph sensing legs after release. Fig. 1(c) shows the optical micrograph of 5×5 sensor array taken through the quartz substrate. The moving mirror region is coated with gold, and the fixed mirror region is coated with aluminum. The difference in the mirror materials comes from fabrication compatibility. Two small dots near the moving region are anchors for bimorph sensing legs.

As shown in Fig. 2, the designed and fabricated sensor can be installed into a physical or chemical environment chamber. Then, a one-to-one imaging setup can be compactly configured outside the chamber. The optical measurement setup consists of a light source, a beam splitter, two lenses, a pinhole, and a CCD, etc. Using this optical setup, the piston motion of each sensor can be simultaneously measured by monitoring the light intensity change on CCD image plane.

To measure the light intensity change due to the temperature change, the fabricated chip is installed on the chip holder, which is temperature controlled by a PID temperature controller (10 mK temperature resolution, Wavelength Electronics Inc.) with a thermistor and serially connected three thermo-electric coolers (TEC). As a light source and a CCD camera, a He-Ne laser (wave length 632.8 nm) and 8 bit CCD camera (COHU Inc.) are used, respectively. Fig. 3 shows

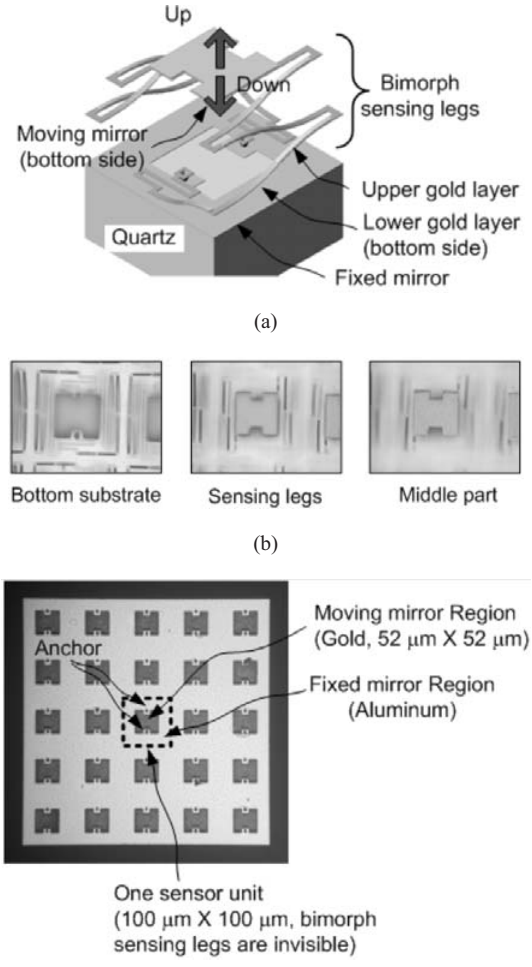

Fig. 1. (a) Bimorph-actuated staggered mirror microsensor. The bimorph sensing legs deform for temperature change and molecular adsorption, then the middle moving part performs piston-type pure vertical motion. (b) Light micrograph taken from the chip top side. Focuses change from the chip substrate to the middle part. (c) Light micrograph taken through quartz substrate. Gold moving region and aluminum fixed mirror region are shown. Two anchors, which are supports for symmetric bimorph sensing legs, are shown also. However, bimorph sensing legs are invisible since it is optically blocked by fixed mirror region.

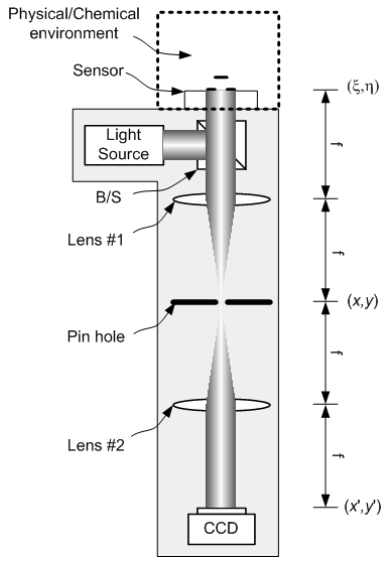

Fig. 2. Interferometric measurement setup. Using this setup, one-to-one imaging of the sensor array is possible. The diffracted light intensity changes of whole sensors or pixels are simultaneously measured by a CCD camera.

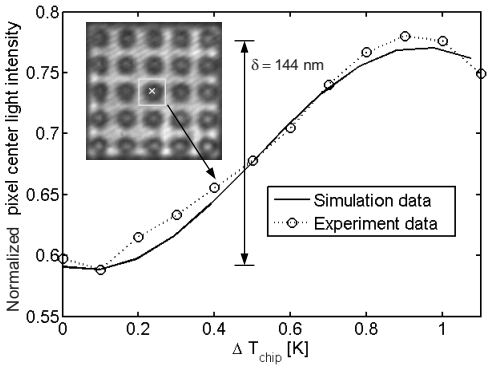

Fig. 3. Pixel center light intensity changes for chip temperature changes.

experimental and simulation results of the normalized intensity changes due to chip temperature changes at an individual sensor. For the chip temperature change of $\Delta T_{chip}{}^{*} = \sim 0.8$ K, the light intensity changes from minimum to maximum. From our previous measurement using WYKO (not through the quartz substrate but from the chip top side), we know the thermo-mechanical sensitivity of the sensor is S_T = 180 nm/K [21]. Therefore the minimum-to-maximum light intensity change corresponds to a 144 nm (= 180 nm/K×0.8 K) deflection of the moving mirror part. Since we used an 8 bit CCD camera and the shift value of light intensity change is 0.168, the deflection

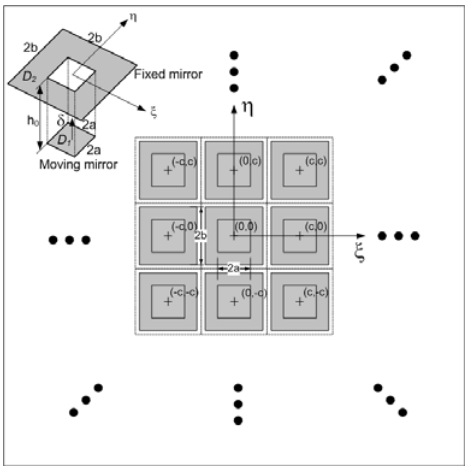

Fig. 4. $(2N+1)\times(2N+1)$ sensor array: pixel (or sensor) size is $2b\times2b$, each sensor has $2a\times2a$ size moving mirror, and the separation of each pixel is c. h_0 is the initial position of the moving mirror (D_1) and δ is the amount of piston motion of the moving mirror.

of 3.35 nm [= 144 nm/ ($2^8\times0.168$)] could be resolved from our current optical setup. The optical simulation using Matlab® was performed by Fourier transform and inverse Fourier transform of light wave function of the sensor array. The experimental results well match the simulation results. In both experimental and simulation results, to get the high contrast of light intensity measurement, the pinhole size adjustment turned out to be critical.

3. Diffraction analysis

Optical diffraction analysis was performed to maximize the sensor sensitivity. Fig. 4 shows the geometry of an individual pixel. Each sensor or pixel size is $2b\times2b$. Each pixel has $2a\times2a$ moving mirror (D_1) and a fixed or reference mirror (D_2). The separation between two pixels is c. h_0 is the initial position of the moving mirror (D_1) and δ is the amount of piston motion of the moving mirror. The phase difference, ϕ, between the moving mirror and the fixed mirror can be expressed as $\phi = 4\pi(h_0 - \delta)/\lambda$. In the sensor array plane, (ξ,η), the wave function, $A_1(\xi,\eta)$, of the light reflected from the fixed mirror can be expressed as

$$A_1(\xi,\eta) = \left[rect\left(\frac{\xi}{2b}\right) rect\left(\frac{\eta}{2b}\right) - rect\left(\frac{\xi}{2a}\right) rect\left(\frac{\eta}{2a}\right) \right] \otimes \underbrace{\sum_{m=-N}^{N}\sum_{n=-N}^{N} \delta(\xi/c - m, \eta/c - n)}_{P(\xi,\eta)} \tag{1}$$

$$= \left[rect\left(\frac{\xi}{2b}\right) rect\left(\frac{\eta}{2b}\right) - rect\left(\frac{\xi}{2a}\right) rect\left(\frac{\eta}{2a}\right) \right] \otimes P(\xi,\eta),$$

where $rect(\cdot)$ is a rectangle function defined by

$$rect(x) = \begin{cases} 1 & |x| < 1/2 \\ 1/2 & |x| = 1/2 \\ 0 & \text{otherwise,} \end{cases} \quad (2)$$

$\delta(\cdot,\cdot)$ is two dimensional Dirac-delta function, $P(\xi,\eta)$ is the periodic function representing the whole sensor array position, and the symbol '⊗' means convolution integral of two functions. Also, the wave function, $A_2(\xi,\eta)$, of the light reflected from the moving mirror can be expressed as

$$A_2(\xi,\eta) = e^{j\phi(\xi,\eta)} \left[rect\left(\frac{\xi}{2a}\right) rect\left(\frac{\eta}{2a}\right) \right] \otimes P(\xi,\eta), \quad (3)$$

where $\phi(\xi,\eta)$ is the phase difference between two light waves from a moving and a fixed mirror. The diffraction pattern of these wave functions can be calculated from the Fourier transform of those as $U_1(f_\xi, f_\eta)$ and $U_2(f_\xi, f_\eta)$.

$$\begin{aligned} U_1(f_\xi, f_\eta) &= \Im\{A_1(\xi,\eta)\} \\ &= \left[4b^2 \operatorname{sinc}(2bf_\xi)\operatorname{sinc}(2bf_\eta) \right. \\ &\quad \left. -4a^2 \operatorname{sinc}(2af_\xi)\operatorname{sinc}(2af_\eta) \right] \\ &\quad \cdot \Im\{P(\xi,\eta)\}, \end{aligned} \quad (4)$$

$$\begin{aligned} U_2(f_\xi, f_\eta) &= \Im\{A_2(\xi,\eta)\} \\ &= \Im\left\{e^{j\phi(\xi,\eta)}\right\} \otimes \\ &\quad \left(\left[4a^2 \operatorname{sinc}(2af_\xi)\operatorname{sinc}(2af_\eta) \right] \cdot \Im\{P(\xi,\eta)\} \right). \end{aligned} \quad (5)$$

In the optical system, the first lens performs the Fourier transform and produces a diffraction pattern corresponding to U_1 and U_2 in its focal plane. We placed a pinhole at the focal plane to block all the primary peaks except for zero-th order peak. Then, Eqs. (4) and (5) can be simplified as

$$U_1'(f_\xi, f_\eta) = 4(b^2 - a^2)\, \Im\{P(\xi,\eta\}, \quad (6)$$

$$U_2'(f_\xi, f_\eta) = 4a^2 \Im\left\{e^{j\phi(\xi,\eta)}\right\} \otimes \Im\{P(\xi,\eta)\}. \quad (7)$$

After the zero-th order peak passes through the pinhole, a second lens is used to perform an inverse Fourier transform, which restores the wave function from the spectral information. In the image plane, (x_i, y_i), the restored wave functions, $U_1'(x_i, y_i)$ and $U_2'(x_i, y_i)$, are expressed as

$$U_1'(x_i, y_i) = \Im\left\{U_1'(f_\xi, f_\eta)\right\} = 4(b^2 - a^2)\, P(x_i, y_i), \quad (8)$$

$$U_2'(x_i, y_i) = \Im\left\{U_2'(f_\xi, f_\eta)\right\} = 4a^2 e^{j\phi(x_i, y_i)}\, P(x_i, y_i) \quad (9)$$

If we note that the function, $P(x_i, y_i)$ is the periodic function representing the sensor array position, the wave functions of each pixel in the array, $U_{s1}'(x_i, y_i)$ and $U_{s2}'(x_i, y_i)$, are expressed as

$$U_{s1}'(x_i, y_i) = 4(b^2 - a^2) \quad (10)$$

$$U_{s2}'(x_i, y_i) = 4a^2 e^{j\phi(x_i, y_i)} \quad (11)$$

Therefore, in the image plane the intensity of each pixel, *I*, can be expressed as

$$\begin{aligned} I &= \left(U_{s1}' + U_{s2}'\right)^* \left(U_{s1}' + U_{s2}'\right) \\ &= 16b^4 \left[\left(1 - (a/b)^2\right)^2 + (a/b)^4 \right. \\ &\quad \left. + 2(a/b)^2 \left(1 - (a/b)^2\right) \cos\phi \right], \end{aligned} \quad (12)$$

where the superscript * implies complex conjugate of the function.

If we note that the phase difference $\phi = 4\pi(h_0 - \delta)/\lambda$ and we define a geometric ratio $\alpha = a/b$, then the above equation can be expressed as

$$I / I_0 = (1-\alpha^2)^2 + \alpha^4 + 2\alpha^2(1-\alpha^2)\cos\frac{4\pi(h_0 - \delta)}{\lambda}, \quad (13)$$

where I_0 is the normalization factor defined as $16b^4$. Eq. (13) indicates that the light intensity will change from minimum-to-maximum for the piston motion amount $\delta^* = \lambda/4 = 158.2$ nm (for $\lambda = 632.8$ nm). The experimental result ($\delta^* = 144$ nm) agrees with this theoretical result within 9 %. If we define opto-mechanical sensitivity as the light intensity change to the amount of piston motion of the moving mirror, then the opto-mechanical sensitivity, β, can be expressed as

$$\begin{aligned} \beta &= \frac{1}{I_0}\frac{dI}{d\delta} \\ &= \frac{8\pi\alpha^2(1-\alpha^2)}{\lambda} \sin\frac{4\pi(h_0 - \delta)}{\lambda}. \end{aligned} \quad (14)$$

From the above equation, it can be easily shown that the opto-mechanical sensitivity can be maximized when the geometric ratio $\alpha^* = 1/\sqrt{2}$. It is interesting that the area of the fixed mirror is the same as that of the moving mirror in the case of the geometric ratio $\alpha = 1/\sqrt{2}$. However, the amount of

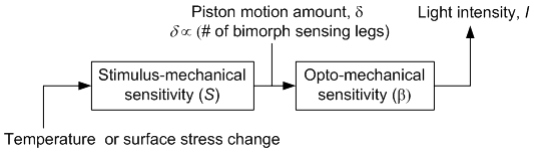

Fig. 5. BASM microsenor block diagram showing serial connection of stimulus-mechanical sensitivity and opto-mechanical sensitivity.

piston motion, δ, can be limited by the geometric constraint, α^*, since it will limit the number of interconnected bimorph sensing legs which can be put into the region between the moving mirror and overall sensor. Fig. 5 shows BASM microsensor block diagram showing the serial connection of stimulus-mechanical sensitivity and opto-mechanical sensitivity. The limited number of bimorph sensing legs will reduce the stimulus-mechanical deformation since it is proportional to the number of bimorph sensing legs. Therefore, to increase overall sensor sensitivity from the environmental stimuli to light intensity change, we need to optimize both the number of bimorph sensing legs and the geometric ratio, α.

4. Conclusions

We performed the interferometric light intensity measurement of a bimorph actuated staggered mirror microsensor, which has piston-type pure vertical motion due to symmetric bimorph sensing legs. Also, optical diffraction analysis was performed, and the optimal geometric ratio of the moving and fixed mirror region was suggested to maximize the opto-mechanical sensitivity. The interferometric measurement setup can be further miniaturized by utilizing fiber-optic coupling process. The coupling of an incoming beam into the core of an optical fiber critically depends on the matching between the beam and the fiber mode profiles, and any change in the incoming beam profile causes fluctuations in the fiber-coupling efficiency. This principle has already been exploited for fiber-optic confocal microscopy [23] and can be applicable to BASM with an appropriate optical system design.

Acknowledgments

The authors would like to thank to Prof. Arun Majumdar and Prof. Roberto Horowitz of UC, Berkeley for the support and useful comments during the optical setup and measurement. This work was supported in part by Seoul Research & Business Development Program (Grant No. 10583) and the new faculty research program 2007 of Kookmin University in Korea.

References

[1] Y. Zhao, M. Y. Mao, R. Horowitz, A. Majumdar and J. Varesi, Optomechanical uncooled infrared imaging system: Design, microfabrication, and performance, *Journal of Microelectromechanical Systems* 11 (2) (2002) 136-146.

[2] S. Cherian, R. K. Gupta and B. C. Mullin, Detection of heavy metal ions using protein-functionalized microcantilever sensors, *Biosensors & Bioelectronics* 19 (5) (2003) 411-416.

[3] H. F. Ji, E. Finot, R. Dabestani, P. Britt, P. Nonnesen and G. Brown, A novel self-assembled monolayer (SAM) coated microcantilever for low level caesium detection, *Chemical Communications* (6) (2000) 457-458.

[4] H. F. Ji, K. M. Hansen, Z. Hu and T. Thundat, Detection of pH variation using modified microcantilever sensors, *Sensors and Actuators B-Chemical* 72 (3) (2001) 233-238.

[5] H. F. Ji and T. Thundat, In situ detection of calcium ions with chemically modified microcantilevers, *Biosensors & Bioelectronics* 17 (4) (2002) 337-343.

[6] L. A. Pinnaduwage, V. Boiadjiev, J. E. Hawk and T. Thomas, Sensitive detection of plastic explosives with self-assembled monolayer-coated microcantilevers, *Applied Physics Letters* 83 (7) (2003) 1471-1473.

[7] L. A. Pinnaduwage, T. Thundat, J. E. Hawk, D. Heddena, P. Britt, E. Houser and S. Stepnowski, Detection of 2,4-dinitrotoluene using microcantilever sensors, *Sensors and Actuators B-Chemical* 99 (2-3) (2004) 223-229.

[8] L. A. Pinnaduwage, H. F. Ji and T. Thundat, oore's law in homeland defense: An integrated sensor platform based on silicon microcantilevers, *IEEE Sensors Journal* 5 (4) (2005) 774-785.

[9] B. Rogers, L. Manning and M. Jones, Mercury vapor detection with a self-sensing, resonating piezoelectric cantilever, *Review of Scientific Instruments* 74 (11) (2003) 4899-4901.

[10] T. Thundat, E. Finot, Z. Hu, R. Ritchie and G. Wu, A. Majumdar, Chemical sensing in Fourier space, *Applied Physics Letters* 77 (24) (2000) 4061-4063.

[11] F. Tian, V. I. Boiadjiev, L. A. Pinnaduwage and T. Thomas, Selective detection of Cr (VI) using a microcantilever electrode coated with a self-assembled monolayer, *Journal of Vacuum Science & Technology A* 23 (4) (2005) 1022-1028.

[12] J. H. Pei, F. Tian and T. Thundat, Glucose biosensor based on the microcantilever, *Analytical Chemistry* 76 (2) (2004) 292-297.

[13] Subramanian, P. I. Oden, S. J. Kennel, K. B. Jacobson, R. J. Warmack, T. Thundat and M. J. Doktycz, Glucose biosensing using an enzyme-coated microcantilever, *Applied Physics Letters* 81 (2) (2002) 385-387.

[14] G. H. Wu, R. H. Datar, K. M. Hansen, T. Thomas, R. J. Cote and A. Majumdar, Bioassay of prostate-specific antigen (PSA) using microcantilevers, *Nature Biotechnology* 19 (9) (2001) 856-860.

[15] G. H. Wu, H. F. Ji, K. Hansen, T. Thomas, R. Datar, R. Cote, M. F. Hagan, A. K. Charkraborty and A. Majumdar, Origin of nanomechanical cantilever motion generated from biomolecular interactions, *Proceedings of the National Academy of Sciences of the United States of America* 98 (4) (2001) 1560-1564.

[16] M. Yue, H. Lin, D. E. Dedrick, S. Satyanarayana and A. Majumdar, A 2-D microcantilever array for multiplexed biomolecular analysis, *Journal of Microelectromechanical Systems* 13 (2) (2004) 290-299.

[17] G. G. Yaralioglu, A. Atalar, S. R. Manalis and C. Quate, Analysis and design of an interdigital cantilever as a displacement sensor, *Journal of Applied Physics* 83 (12) (1998) 7405-7415.

[18] E. B. Cooper, E. R. Post and S. Griffith, High-resolution micromachined interferometric accelerometer, *Applied Physics Letters* 76 (22) (2000) 3316-3318.

[19] N. C. Loh, M. A. Schmidt and S. R. Manalis, Sub-10 cm (3) interferometric accelerometer with nano-g resolution, *Journal of Microelectromechanical Systems* 11 (3) (2002) 182-187.

[20] C. A. Savran, S. M. Knudsen and A. D. Ellington, Micromechanical detection of proteins using aptamer-based receptor molecules, *Analytical Chemistry* 76 (11) (2004) 3194-3198.

[21] S. H. Lim, J. Choi, R. Horowitz and A. Majumdar, Design and fabrication of a novel bimorph microoptomechanical sensor, *Journal of Microelectromechanical Systems* 14 (4) (2005) 683-690.

[22] M. F. Hagan, A. Majumdar and A. K. Chakraborty, Nanomechanical forces generated by surface grafted DNA, *Journal of Physical Chemistry B* 106 (39) (2002) 10163-10173.

[23] J. A. Izatt, M. R. Hee and G. M. Owen, Optical Coherence Microscopy in Scattering Media, *Optics Letters* 19 (8) (1994) 590-592.